Supplementary Material:
Dense Motion Estimation for Natural Phenomenon

In this supplementary material we first provide we provide additional quantitiative and qualitative results for sequences we tested but which are not shown in the main paper. Then we give further mathematical details for the optical flow Optimization (Sec. 3.3 in the main paper).

1 Additional quantitative results

In this section, we provide the full version of Table 1 and Table 2 in the main paper showing the Low Rate Distance(LRD) and High Rate Distance(HRD) errors respectively. Table 1 is a full version of Table 1 in the main paper, and Table 2 is a full version of Table 2 in the main paper. From these full tables, we obtain the comparison error which is defined as followed: we sum the errors across all the sequences for all the methods including the proposed method and other alternatives. The total error sum of the proposed method is used as a reference to obtain the comparison error for all methods, so

$$Comparison\ Error = \frac{Sum\ Error_m}{Sum\ Error_{ours}} - 100\% \tag{1}$$

where m represent different methods in Table 1 and Table 2. As shown in the tables, the proposed method is at least 17% and 31% better than all the alternatives as we claimed in the main paper.

2 Additional qualitative results

In this section, additional qualitative results of motion estimation are given for more sequences of natural phenomena. Figure (2,3,1,4) show a visual comparison on natural phenomena sequences.

As mentioned in the main paper, the test sequences are from our database, public datasets [9, 6, 4], or from the Internet. The qualitative results of motion estimation baselines include Fullflow [3], EpicFlow [8], Class+NL [10], HS [7], BA [1], MDP [11] and Flownet [5].

Figure (3,4) show the motion estimation results and corresponding warping results for all the baselines we compared based on sequences with static or dynamic background from the Internet. Similarly, Figure (2,1) show the results for sequences from the public datasets [9, 6]. Noted that the quantitative results are presented in Table 1 in the main paper.

		Ours	FullFlow	EpicFlow	Class+NL	HS	BA	LDOF	MDP	FlowNet
Our Database	Votex_Speedup	**41.80**	51.90	50.39	51.79	52.60	52.28	50.15	50.21	47.24
	Eddies	**57.23**	68.91	74.07	64.21	65.55	64.06	71.90	68.53	103.4
	Thick_rise	**61.60**	128.12	166.78	100.03	93.48	100.15	160.14	136.48	135.9
	Thin_from_bottom	**37.89**	43.39	43.37	42.44	42.91	42.98	44.08	45.43	39.59
	Thick_Fall_Dissipate	**41.31**	57.67	57.24	57.11	57.78	56.17	56.58	57.39	48.34
	Curved_Fall	**59.35**	80.09	88.60	82.12	83.77	86.03	98.28	82.74	82.50
	Thin_drops_multi	**58.25**	73.32	68.12	65.76	67.16	68.33	64.59	68.14	67.03
	Up_Down_Mix_White	**57.75**	81.24	82.70	69.88	71.46	77.96	80.05	80.14	84.28
	Orange_white_meet	**37.89**	46.56	41.21	42.14	44.94	43.66	41.75	42.79	42.64
	Slanted_surface_pour	**41.00**	59.63	57.73	57.18	56.8	59.58	55.61	56.75	80.11
	Flat_surface_waves	47.63	48.90	52.17	46.21	44.29	45.30	49.99	50.66	**43.37**
	Oscillating_Rising	**48.72**	54.00	53.69	49.80	50.17	49.04	51.41	53.57	51.95
Public Datasets[9, 6, 4]	Steam	**7.38**	8.84	8.27	12.55	12.52	13.01	12.4	13.57	15.47
	Avalanche01	**10.43**	12.29	12.26	12.12	12.57	12.24	12.78	12.64	17.76
	Boil (water)	**13.27**	48.61	18.72	13.91	26.26	25.83	13.94	20.96	42.3
	Fountain01	19.69	26.52	**18.8**	23.67	20.2	20.18	21.39	27.48	22.25
	Fountain02	30.67	61.72	31.72	26.93	34.66	**25.72**	31.3	33.56	27.64
	Forest_fire	**8.37**	8.84	8.39	8.61	10.59	10.45	10.61	9.1	18.85
	Landslide01	**86.08**	87.72	84.94	87.06	89.67	87.82	87.24	86.31	120.2
	Landslide02	88.13	**86.96**	89.43	91.74	89.04	87.49	91.12	91.17	117.7
	Volcano_eruption01	**5.63**	5.82	5.99	5.92	6.89	5.98	5.69	5.97	**5.63**
	Volcano_eruption02	**6.96**	7.22	7.41	7.24	7.54	7.47	7.34	7.58	7.5
	Volcano_eruption03	**7.09**	7.97	7.67	7.99	8.11	8.41	7.65	7.99	7.96
	Waterfall01	**17.86**	19.1	18.97	21.45	20.8	19.89	19.3	17.9	18.33
	Waterfall02	**15.8**	17.76	18	20.02	17.6	18.32	18.14	18.42	18.89
	Waterfall03	**13.97**	15.06	14.91	18.06	18.14	17.88	16.68	14.82	16.00
	Waterfall04	**15.97**	19.12	17.32	19.25	19.19	19.03	17.38	16.84	17.95
Internet	Car_smoke	**8.85**	10.3	10.69	10.64	10.57	10.66	10.58	9.01	10.79
	Fire_smoke	**12.49**	13.21	13.17	12.64	12.81	12.61	12.91	12.68	16.49
	Avalanche02	**12.34**	13.36	13.65	13.38	14.05	13.98	14.24	13.95	15.82
	Train	**11.2**	14.13	14.31	14.28	14.18	14.3	14.08	33.44	16.11
	Fireman	**18.86**	19.42	19.42	19.66	19.52	19.56	19.29	20.72	19.04
	Match_cube	**72.53**	74.65	72.93	80.50	87.40	84.32	77.22	87.88	85.09
	Comparison Error	**0%**	**28%**	**25%**	**17%**	**19%**	**19%**	**25%**	**26%**	**36%**

Table 1: Low Rate Distance (Equation 11 in the main paper, designed for low frame rate video (Public Database and Internet). We compare our method to eight state-of-the-art algorithms using videos from our laboratory, from public datasets, and from the Internet; "Train" is a computer graphic simulation. Bold figures indicate the best performance in each row, we come first in most cases. Data shown $\times 100$ for easy reading. Note that the lower readings show higher accuracy.

*

3 Details of Optical Flow Energy Optimization

In the main paper, we use energy function from [2] for dense flow estimation. The energy function is given as:

$$\begin{aligned} E(\mathbf{v}) &= E_D(\mathbf{v}) + \gamma E_S(\mathbf{v}) \\ &= \int_\Omega \underbrace{\phi(\|f_2(\mathbf{x}+\mathbf{v}) - f_1(\mathbf{x})\|^2)}_{Brightness\ Constancy} + \alpha \underbrace{\phi(\|\nabla f_2(\mathbf{x}+\mathbf{v}) - \nabla f_1(\mathbf{x})\|^2)}_{Gradient\ Constancy} d\mathbf{x} \\ &+ \gamma \int_\Omega \underbrace{\phi(\|\nabla u\|^2 + \|\nabla v\|^2)}_{Smoothness\ Constraint} d\mathbf{x} \end{aligned} \tag{2}$$

		Ours	FullFlow	EpicFlow	Class+NL	HS	BA	LDOF	MDP	FlowNet
Our Database	Votex_Speedup	**25.68**	29.93	29.61	28.78	28.40	29.02	28.53	32.12	31.38
	Eddies	**24.30**	36.78	36.31	35.1	54.91	34.28	37.13	38.35	30.41
	Thick_rise	**26.74**	69.43	72.92	58.54	64.5	53.29	69.16	65.36	61.64
	Thin_from_bottom	**28.03**	40.01	41.28	41.32	38.03	40.6	38.95	38.24	30.99
	Thick_Fall_Dissipate	**24.03**	40.49	42.59	40.87	37.57	38.49	40.51	42.69	29.73
	Curved_Fall	**25.93**	47.75	58.41	44.81	46.75	42.22	53.58	48.77	51.97
	Thin_drops_multi	**32.52**	44.01	51.35	40.41	43.17	36.3	46.06	40.15	34.37
	Up_Down_Mix_White	**27.97**	50.68	52.04	46.24	44.43	43.39	51.63	60.15	42.42
	Orange_white_meet	**21.63**	34	37.13	37.85	36.88	36.2	33.54	34.98	35.28
	Slanted_surface_pour	**20.26**	44.19	41.94	37.41	34.65	34.75	41.92	41.57	39.81
	Flat_surface_waves	**16.87**	31.55	31.14	30.2	27.96	27.33	30.74	30.88	25.49
	Oscillating_Rising	35.37	48.14	53.37	55.29	35.31	30.40	35.48	105.02	**20.95**
Public Datasets[9, 6, 4]	Steam	**12.51**	16.01	15.33	17.40	17.86	16.75	16.36	18.01	18.95
	Avalanche01	**15.33**	28.00	28.53	30.33	27.39	27.58	29.14	28.55	19.75
	Boil_water	**35.87**	40.37	40.95	36.57	36.62	36.45	39.80	28.55	48.15
	Fountain01	**36.67**	61.69	61.56	50.54	47.68	48.99	50.93	50.68	54.53
	Fountain02	**137.1**	165.4	164.5	235.3	177.1	201.0	164.7	164.7	160.9
	Forest_fire	29.81	29.74	31.00	28.27	67.03	78.26	28.66	31.56	**26.24**
	Landslide01	**98.01**	138.9	142.8	127.2	127.2	129.3	139.1	129.7	142.8
	Landslide02	63.17	**56.99**	66.95	78.93	80.47	57.29	77.23	57.94	58.45
	Volcano_eruption01	**15.87**	21.53	21.43	22.70	21.86	21.69	20.96	21.32	20.65
	Volcano_eruption02	**13.79**	20.23	20.40	20.05	19.50	19.86	19.81	19.32	16.16
	Volcano_eruption03	**13.06**	19.97	18.46	19.90	22.06	21.31	19.33	17.96	15.75
	Waterfall01	**30.78**	39.96	40.02	41.38	42.12	45.76	38.76	39.87	42.12
	Waterfall02	39.32	**35.74**	41.78	36.70	37.02	40.39	41.92	39.1	39.69
	Waterfall03	**34.19**	43.06	47.58	42.31	43.80	41.65	42.69	43.08	41.40
	Waterfall04	**32.49**	39.29	39.18	38.70	42.02	61.26	39.84	69.60	39.24
Internet	Car_smoke	**45.26**	49.62	50.17	129.6	116.5	114.3	113.6	98.56	101.4
	Fire_smoke	60.74	120.5	108.2	52.04	60.98	51.90	53.84	60.56	**46.36**
	Avalanche02	**20.56**	29.22	30.98	32.20	23.84	23.48	20.99	20.80	30.45
	Train	**35.76**	83.44	72.45	92.24	91.68	82.13	66.76	150.3	47.11
	Fireman	**59.84**	155.1	167.3	180.8	143.4	180.9	164.9	174.7	124.0
	Match_cube	**57.59**	70.57	71.26	72.75	73.07	72.94	65.23	73.21	73.17
	Comparison Error	**0%**	**49%**	**53%**	**58%**	**51%**	**52%**	**47%**	**61%**	**31%**

Table 2: High Rate Distance (Equation 12) designed for high frame rate video (our database). We compare our method to eight state-of-the-art algorithms using videos from our laboratory, from public datasets, and from the Internet; "Train" is a computer graphic simulation. Bold figures indicate the best performance in each row, we come first in most cases. Data shown $\times 100$ for easy reading. Note that the lower readings show higher accuracy.

where $E_D(\mathbf{v})$ represents the data term consisting the *Brightness* and *Gradient Constancy* in the image space while $E_S(\mathbf{v})$ denotes a smoothness constraint. In the following subsection, we give the full details of energy minimization given the input images f_1 and f_2, as well as the dense initial motion $\mathbf{v}(\mathbf{x})$ (Sec. 3.2 in the main paper).

3.1 Numerical Scheme for Energy Minimization

As mentioned in our main paper, a one-level nested fixed point iterations are applied to minimize our proposed energy. This numerical strategy is used in the recent state-of-the-art work [2]. Here, the similar abbreviations are referred from the original paper:

$$\begin{array}{ll} f_x = \partial_x f_2(\mathbf{x}+\mathbf{v}) & f_{yy} = \partial_{yy} f_2(\mathbf{x}+\mathbf{v}) \\ f_y = \partial_y f_2(\mathbf{x}+\mathbf{v}) & f_z = f_2(\mathbf{x}+\mathbf{v}) - f_1(\mathbf{x}) \\ f_{xx} = \partial_{xx} f_2(\mathbf{x}+\mathbf{v}) & f_{xz} = \partial_x f_2(\mathbf{x}+\mathbf{v}) - \partial_x f_1(\mathbf{x}) \\ f_{xy} = \partial_{xy} f_2(\mathbf{x}+\mathbf{v}) & f_{yz} = \partial_y f_2(\mathbf{x}+\mathbf{v}) - \partial_y f_1(\mathbf{x}) \end{array}$$

At the first phase of energy minimization, a system is built based on Eq. 2 where Euler-Lagrange is employed as follows:

$$\phi'\{f_z^2 + \alpha(f_{xz}^2 + f_{yz}^2)\} \cdot \{f_x f_z + \alpha(f_{xx} f_{xz} + f_{xy} f_{yz})\} - \gamma\phi'(\|\nabla v_1\|^2 + \|\nabla v_2\|^2) \cdot \nabla u = 0 \quad (3)$$

$$\phi'\{f_z^2 + \alpha(f_{xz}^2 + f_{yz}^2)\} \cdot \{f_y f_z + \alpha(f_{yy} f_{yz} + f_{xy} f_{xz})\} - \gamma\phi'(\|\nabla v_1\|^2 + \|\nabla v_2\|^2) \cdot \nabla v = 0 \quad (4)$$

In current system, given the flow field $\mathbf{v}^i = (v_1^i, v_2^i)^T$ from our dense flow interpolation (Sec.3.4), we assume that the solution $\mathbf{v}^{i+1}$ converges on the next level $(i+1)$. Different from the original scheme from [2], our flow field is initialized as $\mathbf{v}^i(\mathbf{x})$ which is the full size dense motion field. In this case, the full size images are used for each iteration of the energy minimization. We have:

$$\begin{aligned} \phi'\{(f_z^{i+1})^2 + \alpha(f_{xz}^{i+1})^2 + \alpha(f_{yz}^{i+1})^2\} \cdot \{f_x^i f_z^{i+1} + \alpha(f_{xx}^i f_{xz}^{i+1} + f_{xy}^i f_{yz}^{i+1})\} \\ -\gamma\phi'(\left\|\nabla v_1^{i+1}\right\|^2 + \left\|\nabla v_2^{i+1}\right\|^2) \cdot \nabla v_1^{i+1} = 0 \end{aligned} \quad (5)$$

$$\begin{aligned} \phi'\{(f_z^{i+1})^2 + \alpha(f_{xz}^{i+1})^2 + \alpha(f_{yz}^{i+1})^2\} \cdot \{f_y^i f_z^{i+1} + \alpha(f_{yy}^i f_{yz}^{i+1} + f_{xy}^i f_{xz}^{i+1})\} \\ -\gamma\phi'(\left\|\nabla v_1^{i+1}\right\|^2 + \left\|\nabla v_2^{i+1}\right\|^2) \cdot \nabla v_2^{i+1} = 0 \end{aligned} \quad (6)$$

Because of the nonlinearity in terms of ϕ', f_*^{i+1}, the system (Eqs. 5, 6) is difficult to solve by linear numerical methods. We apply the first order Taylor expansions to remove these nonlinearity in f_*, which results in:

$$\begin{aligned} f_z^{i+1} &\approx f_z^i + f_x^i dv_1^i + f_y^i dv_2^i \\ f_{xz}^{i+1} &\approx f_{xz}^i + f_{xx}^i dv_1^i + f_{xy}^i dv_2^i \\ f_{yz}^{i+1} &\approx f_{yz}^i + f_{xy}^i dv_1^i + f_{yy}^i dv_2^i \end{aligned}$$

Based on the flow assumption of Brox *et al.* [2] w.r.t. $u^{i+1} \approx u^i + du^i$ and $v^{i+1} \approx v^i + dv^i$ where the unknown flow field on the next level $i+1$ can be obtained using the flow field and its incremental from the current level i. The new system can be presented as follows:

$$
\begin{aligned}
(\phi')^i_D \cdot \{ f^i_x (f^i_z + f^i_x dv^i_1 + f^i_y dv^i_2) \\
+\alpha f^i_{xx}(f^i_{xz} + f^i_{xx} dv^i_1 + f^i_{xy} dv^i_2) + \alpha f^i_{xy}(f^i_{yz} + f^i_{xy} dv^i_1 + f^i_{yy} dv^i_2) \} \\
-\gamma (\phi')^i_S \cdot \nabla (v^i_1 + dv^i_1) = 0
\end{aligned} \tag{7}
$$

$$
\begin{aligned}
(\phi')^i_D \cdot \{ f^i_y (f^i_z + f^i_x dv^i_1 + f^i_y dv^i_2) \\
+\alpha f^i_{yy}(f^i_{yz} + f^i_{xy} dv^i_1 + f^i_{yy} dv^i_2) + \alpha f^i_{xy}(f^i_{xz} + f^i_{xx} dv^i_1 + f^i_{xy} dv^i_2) \} \\
-\gamma (\phi')^i_S \cdot \nabla (v^i_2 + dv^i_2) = 0
\end{aligned} \tag{8}
$$

where the terms $(\phi')^i_D$ and $(\phi')^i_S$ contained ϕ provide robustness to flow discontinuity on the object boundary. In addition, $(\phi')^i_S$ is also regularizer for a gradient constraint in motion space. All of those terms can be detailed as follows:

$$
(\phi')^i_D = \phi' \{ (f^i_z + f^i_x dv^i_1 + f^i_y dv^i_2)^2 + \alpha (f^i_{xz} + f^i_{xx} dv^i_1 + f^i_{xy} dv^i_2)^2 + \alpha (f^i_{yz} + f^i_{xy} dv^i_1 + f^i_{yy} dv^i_2)^2 \} \tag{9}
$$

$$
(\phi')^i_S = \phi' \{ \left\| \nabla (v^i_1 + dv^i_1) \right\|^2 + \left\| \nabla (v^i_2 + dv^i_2) \right\|^2 \} \tag{10}
$$

Although we fixed $\mathbf{v}^i$ in Eqs. 7 8, the nonlinearity in ϕ' leads to the difficulty of solving the system. The inner fixed point iterations are applied to remove this nonlinearity: $dv^{i,j}_1$ and $dv^{i,j}_2$ are assumed to converge within j iterations by initializing $dv^{i,0}_1 = 0$ and $dv^{i,0}_2 = 0$. Finally, we have the linear system in $dv^{i,j+1}_1$ and $dv^{i,j+1}_2$ as follows:

$$
\begin{aligned}
(\phi')^{i,j}_D \cdot \{ f^i_x (f^i_z + f^i_x dv^{i,j+1}_1 + f^i_y dv^{i,j+1}_2) \\
+\alpha f^i_{xx}(f^i_{xz} + f^i_{xx} dv^{i,j+1}_1 + f^i_{xy} dv^{i,j+1}_2) + \alpha f^i_{xy}(f^i_{yz} + f^i_{xy} dv^{i,j+1}_1 + f^i_{yy} dv^{i,j+1}_2) \} \\
-\gamma (\phi')^{i,j}_S \cdot \nabla (v^i_1 + dv^{i,j+1}_1) = 0
\end{aligned} \tag{11}
$$

$$
\begin{aligned}
(\phi')^{i,j}_D \cdot \{ f^i_y (f^i_z + f^i_x dv^{i,j+1}_1 + f^i_y dv^{i,j+1}_2) \\
+\alpha f^i_{yy}(f^i_{yz} + f^i_{xy} dv^{i,j+1}_1 + f^i_{yy} dv^{i,j+1}_2) + \alpha f^i_{xy}(f^i_{xz} + f^i_{xx} dv^{i,j+1}_1 + f^i_{xy} dv^{i,j+1}_2) \} \\
-\gamma (\phi')^{i,j}_S \cdot \nabla (v^i_2 + dv^{i,j+1}_2) = 0
\end{aligned} \tag{12}
$$

This resulting linear system in Eq (11,12) can be solved by common numerical optimization methods such as *Gauss-Seidel* and Successive Over Relaxation (*SOR*). The latter is employed in our implementations. Details for the computation of spatial gradient ∇ and $\|\nabla\|$can be found in Faisal and Barron's work.

References

[1] BLACK, M. J., AND ANANDAN, P. The robust estimation of multiple motions: Parametric and piecewise-smooth flow fields. *Computer vision and image understanding 63*, 1 (1996), 75–104.

[2] BROX, T., BRUHN, A., PAPENBERG, N., AND WEICKERT, J. High accuracy optical flow estimation based on a theory for warping. In *Computer Vision-ECCV 2004*. Springer, 2004, pp. 25–36.

[3] CHEN, Q., AND KOLTUN, V. Full flow: Optical flow estimation by global optimization over regular grids. *arXiv preprint arXiv:1604.03513* (2016).

[4] DERPANIS, K. G., LECCE, M., DANIILIDIS, K., AND WILDES, R. P. Dynamic scene understanding: The role of orientation features in space and time in scene classification. In *Computer Vision and Pattern Recognition (CVPR), 2012 IEEE Conference on* (2012), IEEE, pp. 1306–1313.

[5] DOSOVITSKIY, A., FISCHER, P., ILG, E., HAUSSER, P., HAZIRBAS, C., GOLKOV, V., VAN DER SMAGT, P., CREMERS, D., AND BROX, T. Flownet: Learning optical flow with convolutional networks. In *Proceedings of the IEEE International Conference on Computer Vision* (2015), pp. 2758–2766.

Figure 1: Natural phenomenon sequences from public datasets [9, 6, 4]. Top Row: Input frames. Others: motion field and warping results for proposed method and other baselines.

[6] GHANEM, B., AND AHUJA, N. Maximum margin distance learning for dynamic texture recognition. In *European Conference on Computer Vision* (2010), Springer, pp. 223–236.

[7] HORN, B. K., AND SCHUNCK, B. G. Determining optical flow. In *1981 Technical Symposium East* (1981), International Society for Optics and Photonics, pp. 319–331.

[8] REVAUD, J., WEINZAEPFEL, P., HARCHAOUI, Z., AND SCHMID, C. Epicflow: Edge-preserving interpolation

Figure 2: Natural phenomenon sequences from public datasets [9, 6, 4]. Top Row: Input frames. Others: motion field and warping results for proposed method and other baselines.

of correspondences for optical flow. In *Proceedings of the IEEE Conference on Computer Vision and Pattern Recognition* (2015), pp. 1164–1172.

[9] SHROFF, N., TURAGA, P., AND CHELLAPPA, R. Moving vistas: Exploiting motion for describing scenes. In *Computer Vision and Pattern Recognition (CVPR), 2010 IEEE Conference on* (2010), IEEE, pp. 1911–1918.

[10] SUN, D., ROTH, S., AND BLACK, M. J. Secrets of optical flow estimation and their principles. In *Computer Vision and Pattern Recognition (CVPR), 2010 IEEE Conference on* (2010), IEEE, pp. 2432–2439.

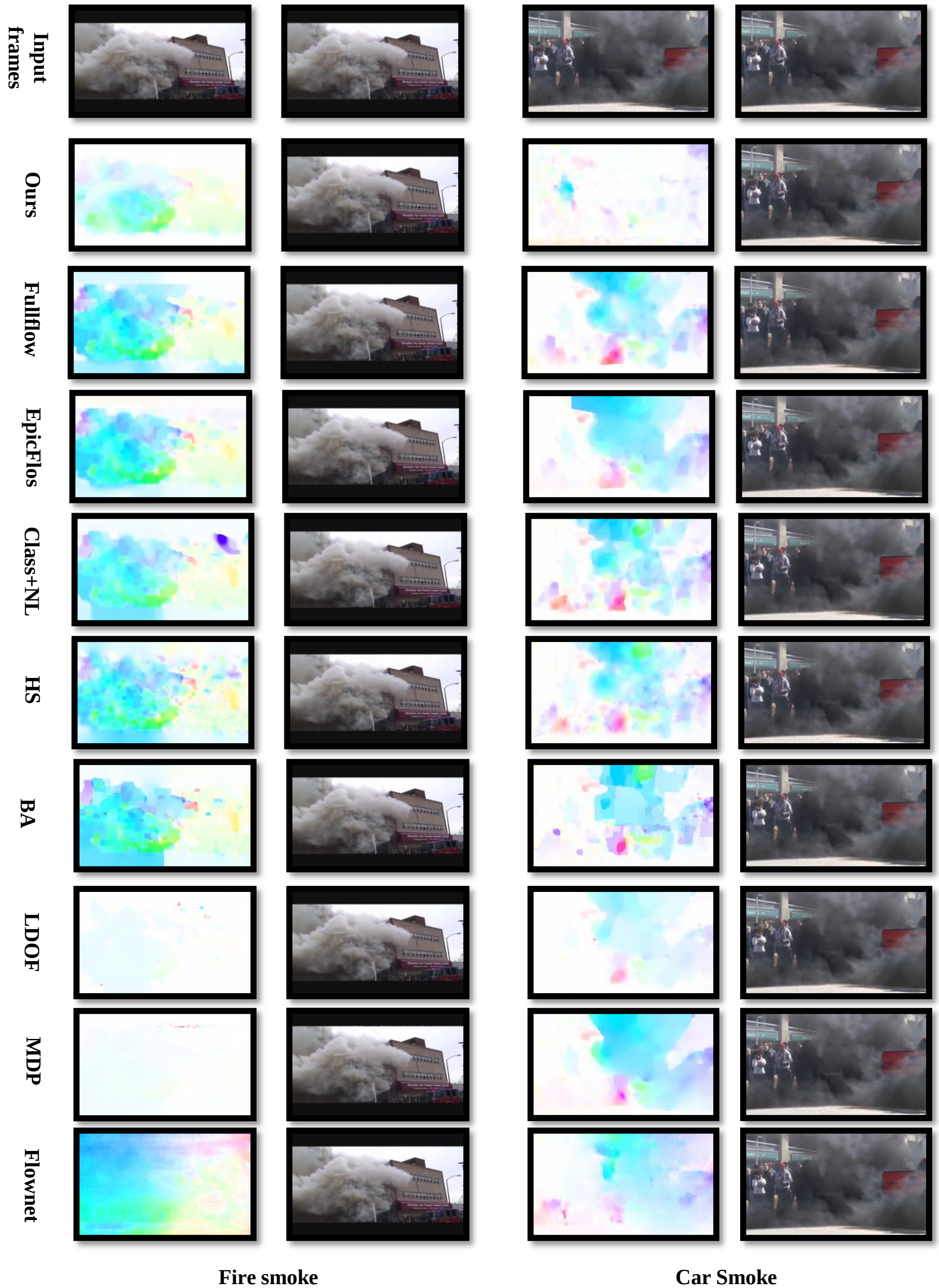

Figure 3: Natural phenomenon sequences from Internet. Top Row: Input frames. Others: motion field and warping results for proposed method and other baselines.

[11] Xu, L., Jia, J., and Matsushita, Y. Motion detail preserving optical flow estimation. *Pattern Analysis and Machine Intelligence, IEEE Transactions on 34*, 9 (2012), 1744–1757.

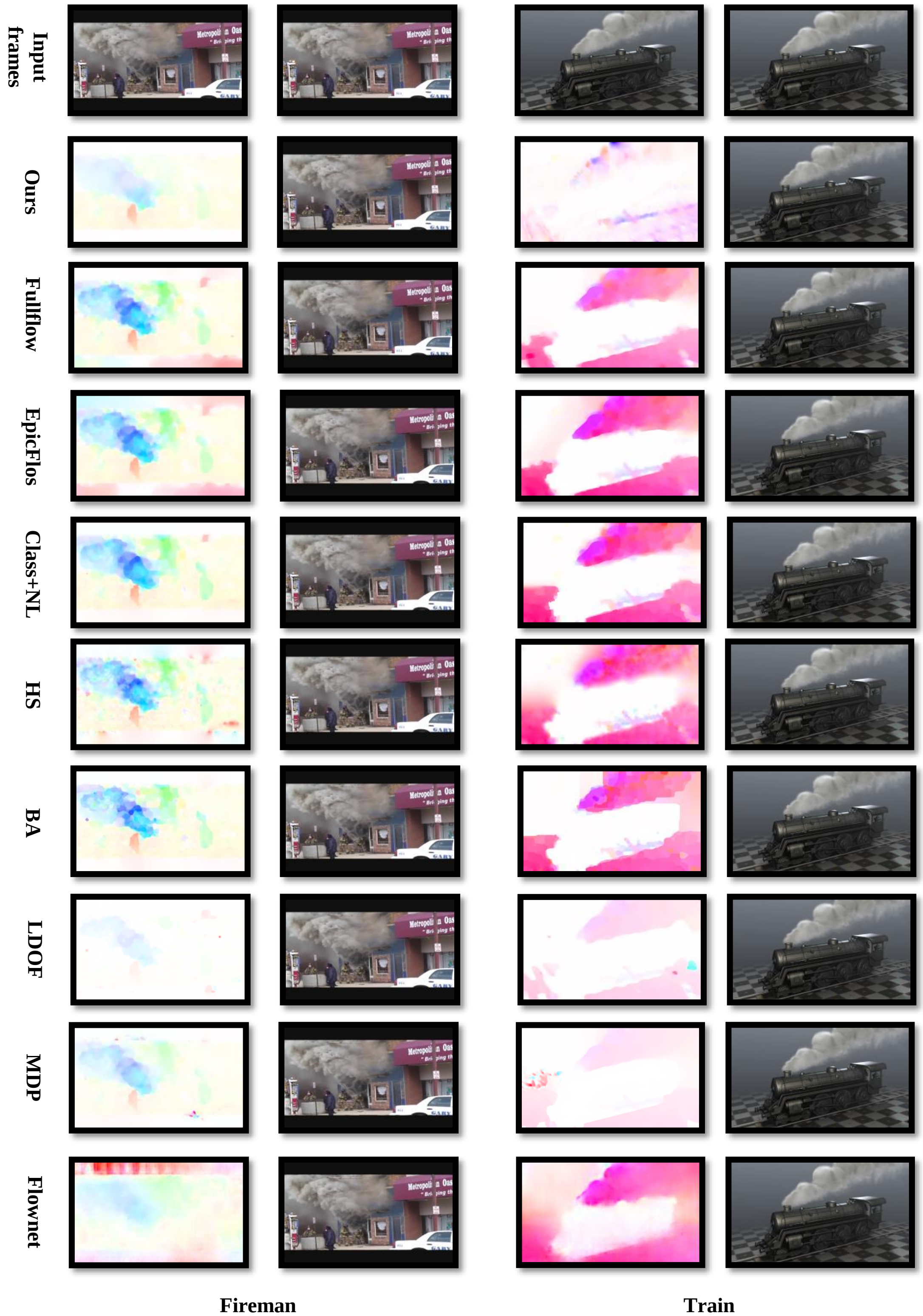

Figure 4: Natural phenomenon sequences from Internet. Top Row: Input frames. Others: motion field and warping results for proposed method and other baselines.